GMR
The Original

GREEN SYNTHESIS OF MULTISCALE POLYMERIC (STARCH/PVA/CUO-NPS) ELECTROSPUN NANOFIBERS FROM *ECTOCARPALES* (MARINE MACROALGAE) EXTRACT: PHYSICOCHEMICAL CHARACTERIZATION AND WOUND HEALING ASSESSMENT ON HACAT CELLS

Vinuritha Kandaswamy[1], Anoosh Golla[2], Radha Mahendran[3], Alagendran Subbarayalu[4], Kaliyamoorthy Dass[5*]

[1]Saveetha Medical College & Hospital (SMCH), Saveetha Institute of Medical and Technical Sciences (SIMATS), Thandalam, Chennai, Tamil Nadu 602105, India. Email: vinu.kandha5@gmail.com
[2]Department of Neurology, Saveetha Medical College and Hospital, Saveetha Institute of Medical And Technical Sciences (SIMATS), Thandalam, Chennai-602105, Tamil Nadu, India. Email: anushyadav2025@gmail.com
[3]Department of Bioinformatics, School of Life Sciences, Vels Institute of Science Technology and Advanced Studies, Pallavaram, Chennai-600117, Tamil Nadu, India. Email: mahenradha@gmail.com; ORCID: https://orcid.org/0000-0003-0711-0336
[4]Saveetha College of Nursing (SCON), Saveetha Institute of Medical and Technical Sciences (SIMATS), Chennai – 602105, Tamil Nadu, India. Email: alagendrans.scon@saveetha.com; ORCID: https://orcid.org/0009-0009-0749-7180
[5*]Natural Product and Vector Control Research Lab, Department of Pharmacology, Saveetha Medical College and Hospital, Saveetha Institute of Medical And Technical Sciences (SIMATS), Thandalam, Chennai-602105, Tamil Nadu, India. Email: dass.smc@saveetha.com;
ORCID: https://orcid.org/0000-0002-4564-3275

ABSTRACT
This study developed novel starch/polyvinyl alcohol (PVA) electrospun nanofibers incorporated with copper oxide nanoparticles (CuO NPs) synthesized via an eco-friendly ultrasound-assisted method using *Ectocarpales* marine macroalgae extract. The physicochemical properties of the nanoparticles and nanoscaffolds were systematically characterized. UV-Vis spectroscopy confirmed the formation of CuO NPs, exhibiting a characteristic absorption edge at 200 nm, while Fourier-transform infrared spectroscopy (FTIR) analysis revealed functional groups from algal biomolecules and Cu–O bonding. X-ray diffraction (XRD) patterns confirmed the monoclinic tenorite phase of CuO NPs, whereas the nanoscaffolds displayed semi-crystalline polymer structures with embedded nanoparticles. Scanning electron microscopy (SEM) imaging showed uniform, bead-free nanofibers with well-dispersed CuO NPs. Thermogravimetric analysis (TGA) demonstrated enhanced thermal stability, with a residual mass of 31.102% attributed to CuO. Dynamic light scattering (DLS) and zeta potential analysis indicated moderate polydispersity (PDI: 0.475) and a positive surface charge (+14.03 mV), suggesting colloidal stability. The wound healing potential was evaluated using a scratch assay on HaCaT keratinocytes. The starch/PVA/CuO-NP nanoscaffolds exhibited superior cell migration, achieving 99.517% wound closure at 100 µg/mL, outperforming both CuO NPs (87.517%) and algal extract (73.517%). These findings highlight the scaffold's exceptional wound healing efficacy, attributed to its nanofibrous structure and bioactive CuO NPs, making it a promising candidate for advanced wound care applications.

KEYWORDS: *Ectocarpales*, Green synthesis, CuO nanoparticles, Starch/PVA/CuO-NPs nanoscaffolds, Wound healing.

1. INTRODUCTION

The increasing demand for advanced wound dressings that promote rapid healing and prevent infections has catalyzed intensive research into bioactive nanomaterials with multifunctional properties [1]. Chronic wounds and burns, often complicated by microbial colonization and delayed tissue regeneration, present a significant clinical challenge worldwide, resulting in increased healthcare costs and patient morbidity [2]. Traditional wound care materials such as gauzes and bandages frequently lack the ability to provide an ideal microenvironment for tissue repair, including moisture retention, antimicrobial protection, and support for cellular proliferation [3]. Hence, the development of innovative biomaterials capable of enhancing the wound healing cascade is critical to improving patient outcomes [4].

Nanotechnology has emerged as a transformative approach in the biomedical field, enabling the design of nanoscale materials that mimic the extracellular matrix (ECM), offer controlled release of therapeutic agents, and exhibit inherent antimicrobial activity [5]. Among these, electrospun nanofibers have gained prominence due to their high surface area-to-volume ratio, porous architecture, and excellent mechanical flexibility, which collectively facilitate oxygen permeability, fluid absorption, and cell attachment [6]. Incorporation of biopolymers like starch and synthetic polymers such as polyvinyl alcohol (PVA) into electrospun mats allows for tuning of physicochemical and biological properties, making these materials suitable scaffolds for wound healing applications.

Starch, a naturally abundant polysaccharide derived from plants, is biodegradable, biocompatible, and possesses inherent film-forming ability [7]. However, its mechanical weakness and poor processability limit standalone applications [8]. To address these drawbacks, starch is often blended with synthetic polymers such as PVA, which provides enhanced mechanical strength, thermal stability, and ease of electrospinning [9]. This synergistic combination can yield nanofibrous

scaffolds with desirable structural integrity and biofunctionality suitable for skin tissue engineering [10]. Furthermore, embedding nanoparticles within these fibers introduces additional functionalities, such as antimicrobial effects and promotion of cellular regeneration, crucial for accelerating wound closure [11].

Copper oxide nanoparticles (CuO NPs) have attracted significant attention in recent years due to their potent antimicrobial, anti-inflammatory, and angiogenic properties, which are beneficial in wound management [12]. CuO NPs exhibit broad-spectrum antimicrobial activity against common pathogens like Staphylococcus aureus and Pseudomonas aeruginosa, bacteria frequently implicated in wound infections [13]. Moreover, copper ions are known to stimulate fibroblast proliferation and promote angiogenesis, thereby enhancing tissue repair [14]. Nonetheless, conventional chemical and physical methods for synthesizing CuO NPs often involve toxic reagents, high energy consumption, and generate hazardous byproducts, limiting their biomedical applicability [15].

In this context, green synthesis methods that utilize biological entities such as plant extracts, algae, or microorganisms have emerged as eco-friendly and sustainable alternatives for nanoparticle production [16]. These biological extracts contain diverse phytochemicals including polyphenols, flavonoids, proteins, and polysaccharides that can act as reducing and stabilizing agents during nanoparticle formation [17]. Marine macroalgae, especially brown algae from the order *Ectocarpales*, represent an underexplored but rich source of bioactive compounds suitable for green synthesis [18]. These seaweeds thrive in saline environments, accumulating unique secondary metabolites such as fucoidans, phlorotannins, and sulfated polysaccharides, which possess antioxidant, antimicrobial, and anti-inflammatory activities [19]. Utilizing extracts from *Ectocarpales* for CuO NP synthesis not only leverages the intrinsic biological activity of the algae but also aligns with sustainable and renewable material development [20].

The use of ultrasound-assisted extraction further enhances the yield and efficiency of phytochemical recovery from marine algae [21]. Ultrasonication promotes cell wall disruption and increases solvent penetration, leading to improved extraction of bioactive compounds in shorter durations with reduced solvent consumption [22]. Integrating ultrasound-assisted extraction with green nanoparticle synthesis provides a novel, rapid, and environmentally benign route to generate biologically functional CuO NPs [23].

Embedding green-synthesized CuO NPs into starch/PVA electrospun nanofibers offers a promising strategy to fabricate multifunctional wound dressings that combine the biocompatibility of the polymeric matrix with the antimicrobial and regenerative properties of nanoparticles [24]. Electrospinning allows uniform dispersion of CuO NPs within the nanofibrous scaffold, maintaining nanoscale fiber morphology and enhancing surface interactions with cells [25]. These hybrid nanofibers can serve as an effective barrier against microbial invasion, maintain a moist wound environment, and stimulate cellular migration and proliferation necessary for healing [26].

Although prior studies have reported on the synthesis of metal oxide nanoparticles using terrestrial plant extracts and their incorporation into polymeric matrices [27], the specific use of marine macroalgae from the *Ectocarpales* order for ultrasound-mediated green synthesis of CuO NPs remains scarcely explored. Furthermore, the fabrication of starch/PVA electrospun nanofibers embedded with such marine-derived CuO NPs and evaluation of their wound healing potential provides a novel contribution to the field of marine biopolymer-based nanomaterials for tissue engineering [28].

This study aims to bridge this knowledge gap by developing and characterizing starch/PVA electrospun nanofibers incorporated with CuO NPs synthesized via an ultrasound-assisted green method using *Ectocarpales* marine macroalgae extract. The physicochemical properties of the composite nanofibers, including morphology, crystallinity, thermal stability, and colloidal characteristics, are comprehensively investigated [29]. Moreover, the biological efficacy of these hybrid scaffolds is assessed using in vitro wound healing assays to evaluate their ability to promote keratinocyte migration and wound closure [30]. The findings are anticipated to contribute to the design of sustainable, biocompatible, and multifunctional nanofibrous wound dressings leveraging marine bioresources and green nanotechnology [31].

MATERIALS AND METHODS

2.1. Chemicals and materials

Marine brown algae from the *Ectocarpales* order were harvested along the Rameswaram coastline in Tamil Nadu, serving as a renewable biosource for the eco-friendly synthesis of CuO NPs. Copper (II) sulfate pentahydrate ($CuSO_4 \cdot 5H_2O$, Sigma-Aldrich) was utilized as the precursor salt. PVA with an average molecular weight of 145,000 and commercially available starch were employed to fabricate electrospun nanofiber mats using a HOLMARC HO-NFES-040 electrospinning unit. All other solvents and reagents, sourced from Sigma-Aldrich and Merck, were of analytical grade and used without further purification. Analytical techniques included UV-visible spectroscopy, Fourier-transform infrared spectroscopy (FTIR), X-ray diffraction (XRD) using a Bruker D8 Advance, Scanning electron microscopy (SEM) via JEOL JSM-IT800, zeta potential analysis using a Malvern Zetasizer Ultra, and thermal analysis with a PerkinElmer Thermogravimetric analysis (TGA) 8000. Wound healing effects were assessed using standard evaluation protocols.

2.2. Collection and preparation of *Ectocarpales* algae

Brown algae from the *Ectocarpales* group were manually collected from the intertidal zone along the Rameswaram coast. To remove physical contaminants, samples were initially washed with tap water to eliminate sand and debris, followed by rinsing with distilled water for further purification. Approximately 100 g of cleaned algae were chopped into small fragments and subjected to shade drying at ambient temperature (~28°C) for 14 days. The dried algal material was ground into a fine powder using a mechanical grinder and stored in moisture-free airtight containers for subsequent use.

2.3. Ultrasound-assisted extraction of bioactive compounds

To extract phytochemicals, 2 g of algal powder was suspended in 50 mL of Milli-Q water in a sterilized beaker. This mixture was placed in a LABQUEST ultrasonic bath (Borosil; Serial No. 941032329018) at 60°C for 45 minutes.

Ultrasonication disrupted algal cell walls, enhancing the release of bioactive components. The solution was then filtered using Whatman No. 1 paper under sterile conditions. The resulting filtrate was either stored at 10°C for immediate use or freeze-dried to obtain a stable powdered extract for future applications[32, 33].

2.4. Green synthesis of CuO NPs

The algal extract functioned as both a reducing and stabilizing agent for synthesizing CuO NPs. A 0.1 M aqueous solution of $CuSO_4 \cdot 5H_2O$ (50 mL) was combined with 10 mL of algal extract (prepared by dissolving 10 mg of lyophilized powder in 10 mL of Milli-Q water) in a 5:1 ratio. The mixture was stirred magnetically at 650 rpm and maintained at 60°C for 2 hours. The formation of nanoparticles was indicated by a color change from deep blue to bluish-green. The resultant solution was washed three times with double-distilled water to remove residual biomolecules and salts. Lyophilization for 48 hours yielded a fine CuO nanopowder for downstream applications[34].

2.5. Fabrication of starch/PVA nanofibers embedded with CuO NPs

To fabricate hybrid nanofibers, 15% (w/w) PVA was dissolved in distilled water under consistent heat and stirring. Once fully solubilized, 100 mg each of starch and synthesized CuO NPs were added and stirred at 50°C for 2.5 hours to ensure even dispersion. The polymer blend was transferred to a syringe equipped with a 0.84 mm needle and electrospun using a HOLMARC HO-NFES-040 system. The optimized conditions included an applied voltage of 11.5 kV, a nozzle-to-collector gap of 12.3 cm, and a flow rate of 0.4 mL/h. The nanofibers were collected on aluminum foil for 6–8 hours at ambient temperature, forming uniform fibrous mats[35-37].

2.6. Physicochemical characterization methods

2.6.1. UV-visible spectral analysis

A VIS SPEC V-730 spectrophotometer was employed to determine the optical absorption characteristics of the algal extract, CuO NPs, and composite nanofibers. Absorbance spectra were recorded from 200 to 800 nm, using deionized water as the blank reference[38].

2.6.2. FT-IR spectroscopic analysis

FT-IR spectra were acquired using a PerkinElmer Spectrum Two spectrometer in ATR mode, over a wavenumber range of 4000–400 cm^{-1}. The resolution was set at 4 cm^{-1}, and each spectrum was averaged over 64 scans to improve signal clarity and identify functional groups related to synthesis and scaffold structure[39].

2.6.3. XRD analysis

XRD was conducted on a Bruker D8 Advance diffractometer using CuKα radiation ($\lambda = 1.5406$ Å), operated at 40 kV and 40 mA. Data acquisition ranged from $2\theta = 5°$ to 90° at a scan step size of 0.029649°, revealing crystalline structures within nanoparticles and composites[40].

2.6.4. SEM analysis

Surface morphology of CuO NPs and nanofiber mats was examined via a JEOL JSM-IT800 SEM. Prior to imaging, samples were gold-coated to enhance conductivity and resolution. SEM was used to analyze fiber uniformity, particle dispersion, and topographical features[41].

2.6.5.TGA

Thermal properties were evaluated using a PerkinElmer TGA 8000. Approximately 5 mg of each sample was heated from room temperature to 550°C at a rate of 15°C/min under a nitrogen atmosphere. Thermal stability and decomposition patterns were recorded[42].

2.6.6. Particle size and zeta potential analysis

A Malvern Zetasizer Ultra was employed to assess the hydrodynamic diameter and zeta potential of CuO NPs using dynamic and electrophoretic light scattering. These parameters provided insight into colloidal stability and particle dispersion[43]. All physicochemical data are available at Mendeley Data (DOI: 10.17632/m7jzmb7mr9.1).

2.7. Wound healing (scratch) assay

A scratch assay was performed to assess the migratory response of HaCaT keratinocyte cells after exposure to various test formulations, including algal extract, CuO NPs, and starch/PVA/CuO-NPs composite nanoscaffolds. Cells were cultured in 12-well plates at a seeding density of 2×10^5 cells per well using Dulbecco's Modified Eagle Medium (DMEM) supplemented with 10% fetal bovine serum (FBS) and 1% penicillin-streptomycin. Incubation was carried out at 37 °C in a humidified incubator with 5% CO_2 until a uniform monolayer formed. A sterile 200 µL pipette tip was employed to create a consistent linear scratch across the center of each well to mimic a wound. Following this, phosphate-buffered saline (PBS) was used to gently rinse the wells to eliminate detached cells. Cells were then treated with the designated test formulations—algal extract, CuO NPs, and starch/PVA/CuO-NPs nanoscaffolds—at varying concentrations (6.25, 12.5, 25, 50, and 100 µg/mL) in serum-free DMEM. Control wells without any treatment were included for comparison. Wound closure was documented at 0, 24, and 48 hours using an inverted phase-contrast microscope. The extent of cell migration across the scratched region was analyzed with ImageJ software, and the percentage of wound closure was calculated to evaluate the comparative healing potential of the treatments at different doses [44].

2.8. Statistical analysis

All experimental outcomes were statistically evaluated using SPSS version 25.0 and GraphPad Prism version 9.0. Data from triplicate trials were expressed as mean ± standard deviation. One-way ANOVA was used to determine statistical differences among groups, followed by post-hoc tests such as Tukey's or Dunnett's where relevant. A p-value < 0.05 was

deemed statistically significant. Correlations were analyzed using Pearson's coefficient. The Shapiro–Wilk test assessed normality; if violated, data underwent logarithmic transformation. All conclusions were drawn at a 95% confidence level to ensure robustness and reproducibility [45].

RESULTS

3.1. UV–visible spectroscopic characterization

The UV–Visible absorption profiles (Figure 1) of the *Ectocarpales* extract and the biosynthesized CuO NP were measured using a JASCO UV-VIS spectrophotometer (Model V-730) over the wavelength range of 200 to 800 nm, with deionized water as the blank. The algal extract displayed a broad absorption region between 200 and 400 nm, featuring a pronounced peak around 300 nm with an absorbance of 0.93687. This peak corresponds to π-π* electronic transitions typically associated with phenolic compounds, flavonoids, and chlorophyll derivatives commonly present in marine algae. From 400 to 800 nm, the absorbance steadily decreased, indicating minimal light absorption in the visible spectrum, consistent with the limited extent of conjugated systems in the extract. Conversely, the CuO NPs exhibited a sharp absorption edge at 200 nm with an absorbance value of 0.53295, indicative of their intrinsic semiconductor bandgap and potential surface plasmon resonance effects. The absorbance decreased progressively at longer wavelengths, a characteristic feature of semiconductor nanomaterials. These distinct absorption patterns between the organic extract and the inorganic CuO NPs confirm their differing chemical compositions and validate the successful formation of CuO NPs with unique optical properties [45, 46].

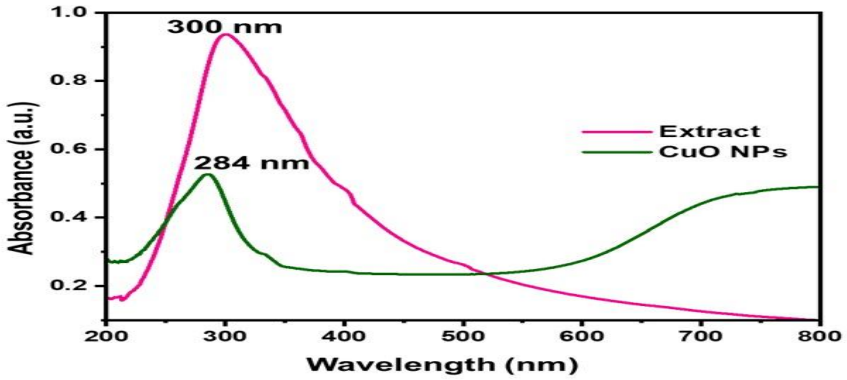

Figure 1. UV–Visible Spectroscopy analysis of algae extract and CuO NPs

3.2. FT-IR spectral analysis

FT-IR spectra (Figure 2) were recorded for CuO NPs and their nanoscaffold composites using a PerkinElmer Spectrum Two instrument with ATR mode over 4000 to 400 cm^{-1}, at 4 cm^{-1} resolution and 64 scans. The CuO NPs displayed major absorption bands at 3216 cm^{-1} attributed to O–H stretching vibrations from adsorbed water molecules, and a band near 1511 cm^{-1} likely associated with C=O stretching or aromatic ring vibrations. A distinct band at 860 cm^{-1} was assigned to Cu–O stretching, confirming the presence of copper oxide and residual organic groups from the green synthesis process. The nanoscaffold spectrum showed broader, more complex features with a prominent peak at 3298 cm^{-1} due to O–H and/or N–H stretching, typical for polymeric matrices. A band observed at 2107 cm^{-1} indicated the presence of C≡N or conjugated C=C=N groups. The peaks at 1652 cm^{-1} and 1327 cm^{-1} corresponded to C=O stretching and O–H or C–N bending vibrations, respectively. Additional bands at 840 and 607 cm^{-1} suggested glycosidic bonds and interactions between the inorganic CuO and polymer chains. These spectral signatures confirm both the formation of CuO NPs and their successful embedding into the polymer scaffold [47-51].

3.3. XRD analysis

XRD patterns (Figure 3) for CuO NPs and nanoscaffolds were acquired using a Bruker D8 Advance diffractometer with CuKα radiation (λ = 1.5406 Å) at 40 kV and 40 mA. The scanning range was 2θ = 5° to 90° with a step size of 0.029649°. The CuO NPs exhibited 25 distinct diffraction peaks, with the most intense reflections at 26.201° (d = 3.398 Å), 20.312° (d = 4.369 Å), and 36.148° (d = 2.483 Å), which correspond to the monoclinic tenorite phase (JCPDS No. 05-0661). The narrow and sharp peaks indicated a highly crystalline structure. The nanoscaffold XRD pattern showed 14 peaks dominated by broad signals at 21.199° (d = 4.188 Å) and 30.844° (d = 2.897 Å), characteristic of a semi-crystalline polymer network, calculated to contain 15.9% crystalline and 84.1% amorphous content. Peak broadening and increased full-width at half maximum (FWHM) suggested reduced orderliness due to CuO NP dispersion within the polymer. The absence of overlapping peaks confirmed the purity and structural stability of both the CuO NPs and their composite scaffolds [52-56].

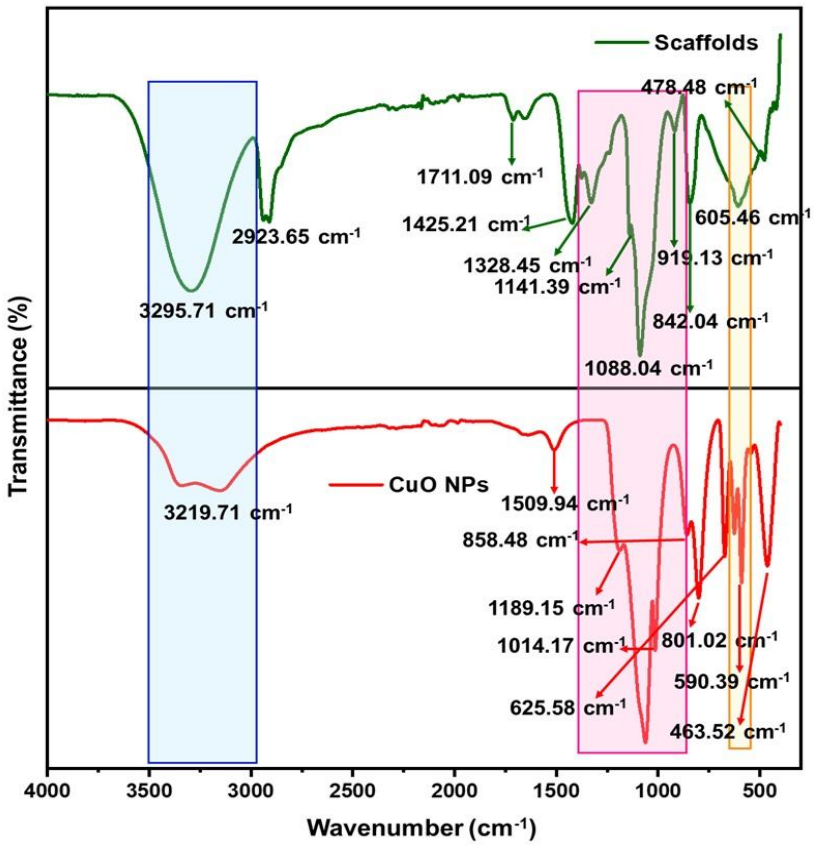

Figure 2. FTIR analysis of CuO NPs and starch/PVA/CuONPs nanoscaffolds

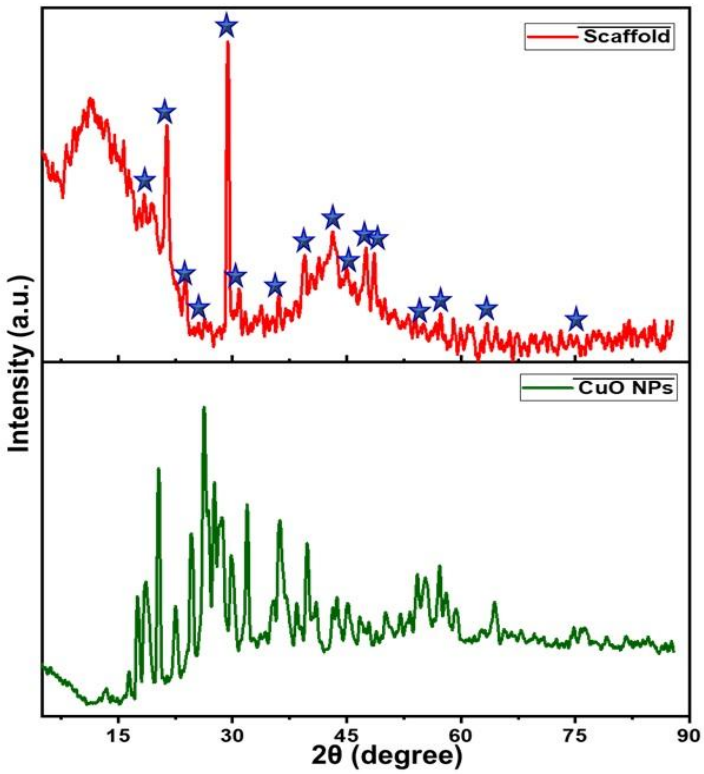

Figure 3. XRD analysis of CuO NPs and starch/PVA/CuONPs nanoscaffolds

3.4. SEM analysis

SEM images (Figure 4) collected via a JEOL JSM-IT800 NANO SEM revealed the morphology of CuO NPs and electrospun nanofibrous scaffolds. The CuO NPs appeared predominantly spherical to slightly irregular, with particle sizes ranging from 50 to 200 nm. Mild agglomeration was visible, attributed to the high surface energy of the nanoparticles, yet individual particles remained identifiable. The nanoscaffolds exhibited a highly porous, interconnected fibrous network with fiber diameters between 70 and 90 nm. The fibers were mostly smooth, with occasional bead-like structures indicating

well-optimized electrospinning parameters. Bright spots seen on the fiber surfaces were identified as embedded CuO NPs, confirming their uniform distribution within the scaffold matrix. This hierarchical porous architecture combined with well-dispersed nanoparticles suggests the scaffolds' promising suitability for biomedical applications such as tissue engineering and wound repair, with minimized nanoparticle clustering [57].

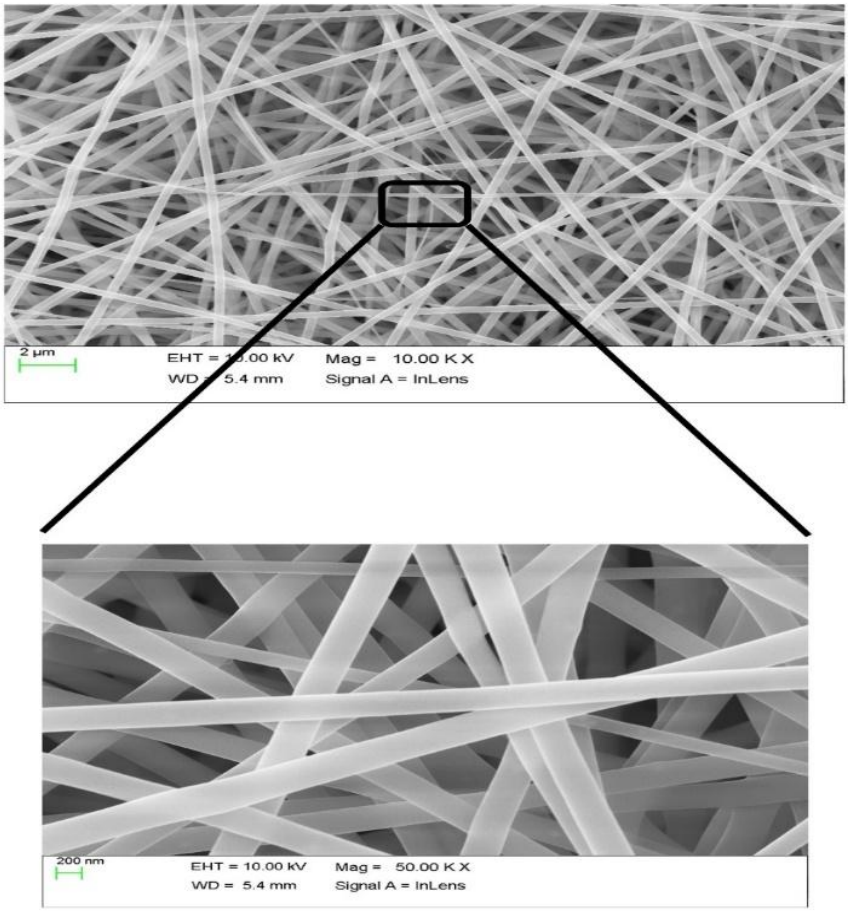

Figure 4. SEM analysis of starch/PVA/CuONPs nanoscaffolds

3.5. TGA analysis

TGA of the nanoscaffolds (Figure 5) was performed using a PerkinElmer TGA 8000 system. A 1.012 mg sample was heated from room temperature up to 600°C under nitrogen flow at a heating rate of 15°C/min. The thermogram showed a multi-stage degradation profile. An initial weight loss of 3.581% below 100°C was attributed to the evaporation of moisture and solvents. The primary thermal degradation occurred at 336.92°C, corresponding to the breakdown of the polymer matrix components such as starch or PVA. Complete decomposition was observed by 400.84°C, with a residual mass of 31.102%, attributed to the thermally stable CuO NPs. The relatively high decomposition temperature and significant residue indicate enhanced thermal stability of the composite nanoscaffold, suggesting its suitability for applications requiring thermal resistance. These findings demonstrate the composite's structural robustness and strong nanoparticle-polymer integration [58].

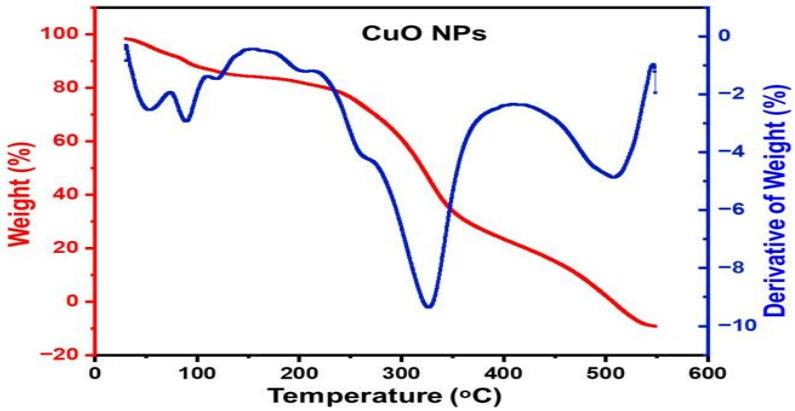

Figure 5. TGA analysis of starch/PVA/CuONPs nanoscaffolds

3.6. DLS and zeta potential

DLS and zeta potential measurements were conducted using a Malvern Zetasizer Ultra to assess the hydrodynamic size and surface charge of the CuO NPs. The DLS data revealed an average hydrodynamic diameter (Z-average) of 79.8 nm

(Figure 6) with a polydispersity index (PDI) of 0.475, indicating moderate particle size distribution. Zeta potential analysis (Figure 7) showed an average surface charge of +14.03 mV, with two main peaks at +10.94 mV and +28.06 mV. The positive charge likely originates from organic capping agents remaining from the green synthesis process. The nanoparticle suspension exhibited conductivity of 0.1179 mS/cm and a quality factor of 2.084, indicative of reasonable colloidal stability. Although some larger aggregates were detected, the CuO NPs demonstrated satisfactory dispersibility and surface charge stability, which are essential properties for their effective application in biomedical and environmental fields. These physical parameters provide valuable insights into nanoparticle behavior in suspension [59].

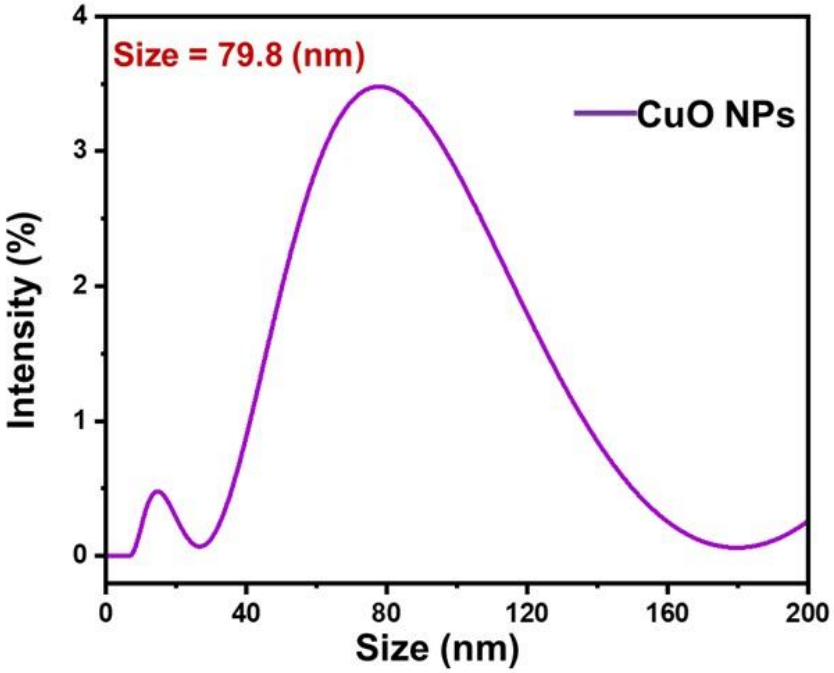

Figure 6. Particle size analysis of CuO NPs

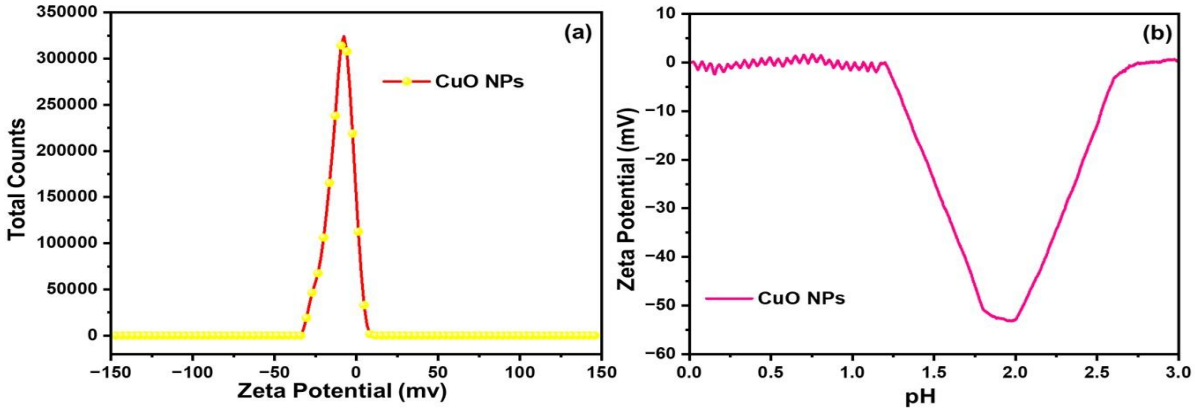

Figure 7. Zeta potential analysis of CuO NPs

3.7. Wound healing (scratch) assay

The wound healing (scratch) assay demonstrated significant variations in the migratory behavior of HaCaT keratinocyte cells after 48 hours of treatment with algal extract, CuO NPs, and starch/PVA/CuO-NPs nanoscaffolds. At the lowest concentration (6.25 µg/mL), the algal extract exhibited a wound closure rate of 36.517%, while CuO NPs and nanoscaffolds showed higher rates of 44.517% and 51.517%, respectively. This indicates that the nanoscaffolds were the most effective at promoting cell migration at this concentration, followed by CuO NPs and then the algal extract. As the concentration increased to 12.5 µg/mL, the wound closure rates further improved. The algal extract achieved 43.517% closure, CuO NPs reached 50.517%, and the nanoscaffolds showed the highest efficacy at 66.517%. This trend continued at 25 µg/mL, where the algal extract, CuO NPs, and nanoscaffolds resulted in 54.517%, 66.517%, and 77.517% wound closure, respectively. The data clearly highlights the superior performance of the nanoscaffolds in enhancing cell migration compared to the other treatments.

At higher concentrations (50 and 100 µg/mL), the differences in efficacy became even more pronounced. The algal extract yielded 64.517% and 73.517% wound closure, while CuO NPs achieved 68.517% and 87.517%. Notably, the nanoscaffolds outperformed both, with closure rates of 83.517% and 99.517% at these concentrations. The near-complete wound closure observed with the nanoscaffolds at 100 µg/mL suggests their exceptional potential in accelerating wound healing.

The starch/PVA/CuO-NPs nanoscaffolds consistently exhibited the highest wound healing activity across all tested concentrations, followed by CuO NPs and then the algal extract. These results underscore the promising role of

nanoscaffolds in promoting keratinocyte migration and wound repair, making them a strong candidate for further development in wound healing applications [60].

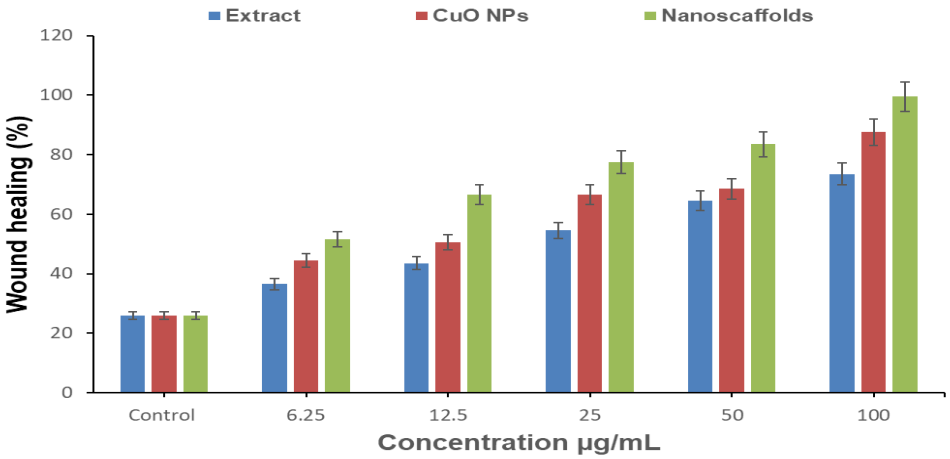

Figure 8. Wound healing potential of algal extract, CuO NPs and starch/PVA/CuO-NPs nanoscaffolds

DISCUSSION

The UV–Visible spectroscopic analysis provided clear evidence of the successful biosynthesis of CuO NPs (NPs) from the *Ectocarpales* algal extract. The broad absorption peak around 300 nm in the algal extract corresponds well with the characteristic electronic transitions of phenolic compounds, flavonoids, and chlorophyll derivatives, which are known to play key roles as natural reducing and stabilizing agents in nanoparticle synthesis. This absorption pattern indicates the presence of various bioactive molecules capable of facilitating the reduction of copper ions and subsequent nanoparticle formation. In contrast, the distinct sharp absorption edge at 200 nm observed for CuO NPs is typical of semiconductor materials, reflecting their bandgap energy and unique optical properties. This difference between the extract and nanoparticles confirms not only the formation of CuO NPs but also the alteration in electronic structure due to the inorganic nature of copper oxide, distinguishing them clearly from the organic matrix of the extract [61].

FT-IR spectroscopy further corroborated the successful synthesis and incorporation of CuO NPs within the nanoscaffold matrix. The CuO NPs exhibited characteristic peaks such as the Cu–O stretching vibration near 860 cm^{-1}, a definitive marker for copper oxide presence. The observed bands related to O–H and C=O groups suggest residual organic moieties from the algal extract capping the nanoparticles, which is typical in green synthesis methods. The nanoscaffold spectrum showed broader and more complex bands, indicating the integration of the polymeric matrix—likely starch and PVA—with the embedded nanoparticles. The presence of functional groups such as O–H/N–H stretching and C=O stretching highlights the polymeric nature, while additional bands indicative of glycosidic bonds and possible interactions between the polymer and CuO confirm a stable composite formation. Such chemical interactions are essential for the physical integrity and functional properties of the nanoscaffold, ensuring effective nanoparticle immobilization and sustained bioactivity [62-65].

XRD analysis revealed that the CuO NPs possess a highly crystalline monoclinic tenorite structure, with well-defined sharp peaks that confirm high crystallinity and purity. This structural confirmation is critical since the crystallinity of metal oxide nanoparticles directly impacts their physicochemical and biological activities. When embedded within the nanoscaffold, however, the diffraction pattern showed broader peaks, indicating a semi-crystalline polymer network with a large amorphous fraction. This peak broadening and reduced crystallinity are expected outcomes when rigid nanoparticles are dispersed within a flexible polymer matrix. Importantly, the absence of overlapping or impurity peaks affirms that the nanocomposite formation did not compromise the individual components' structural integrity. The reduced crystallinity in the composite likely enhances flexibility and mechanical resilience, beneficial for biomedical scaffold applications where elasticity and structural support are required [66].

Morphological examination via SEM provided insight into the physical architecture and distribution of the nanoparticles and polymer fibers. The CuO NPs exhibited predominantly spherical to slightly irregular shapes with sizes consistent with nanoscale dimensions. Although mild agglomeration was noted, it did not appear severe enough to affect particle individuality, a common challenge due to high surface energy in nanoparticles. The nanoscaffold morphology was characterized by a highly porous fibrous network with uniform fiber diameters, indicating optimized electrospinning parameters. The visible bright spots on the fibers—attributed to embedded CuO NPs—suggest effective nanoparticle dispersion and immobilization within the scaffold. This homogeneous distribution is crucial for ensuring consistent biological activity and avoiding localized nanoparticle clusters that could lead to cytotoxicity or uneven scaffold properties. The fibrous porous architecture is advantageous for tissue engineering, as it mimics the ECM and allows nutrient diffusion and cell infiltration, supporting wound healing and regeneration [67, 68].

TGA confirmed the enhanced thermal stability of the nanoscaffold composite. The initial weight loss corresponds to the evaporation of moisture and residual solvents, a typical phenomenon in polymeric materials. The primary degradation temperature near 337°C aligns with the decomposition of organic polymer components such as starch and PVA. Notably, the residual mass of over 31% at high temperature is indicative of the robust presence of thermally stable CuO NPs. This improved thermal stability suggests strong interaction between the nanoparticles and the polymer matrix, which can enhance the composite's durability under physiological or sterilization conditions. Such thermal robustness is an important consideration for biomedical materials, as it ensures scaffold integrity during storage and application [69].

DLS and zeta potential measurements revealed that the CuO NPs have an average hydrodynamic size around 80 nm, which is consistent with SEM findings and suitable for biomedical applications requiring nanoscale particles. The moderate polydispersity index indicates a reasonable size distribution, though some aggregation may exist. The positive zeta potential values suggest that the nanoparticles carry a surface charge likely due to organic capping agents from the algal extract, which contributes to colloidal stability by electrostatic repulsion. This surface charge is critical in biomedical contexts, as it influences cellular uptake, interaction with biomolecules, and dispersion stability in physiological fluids. The moderate conductivity and quality factor further support the colloidal stability and suitability of these nanoparticles for suspension-based applications [70].

The wound healing scratch assay results demonstrated the practical biomedical potential of the synthesized nanoscaffolds. The superior wound closure rates observed with starch/PVA/CuO-NPs nanoscaffolds across all concentrations compared to both the pure CuO NPs and the algal extract alone highlight the synergistic effect of combining nanoparticles with a polymeric scaffold. The nanoscaffolds' porous, bioactive architecture likely promotes keratinocyte migration more effectively, accelerating the wound closure process. This enhancement can be attributed to the controlled release of CuO NPs and bioactive compounds from the scaffold, which may stimulate cellular proliferation and migration, reduce oxidative stress, and provide antimicrobial effects. The nearly complete wound closure at the highest concentration underscores the scaffold's potential as an effective wound healing material, offering improved efficacy over nanoparticle suspensions or crude extracts. These findings support further development and optimization of such nanocomposites for regenerative medicine and tissue engineering applications [71].

CONCLUSION

This study successfully demonstrated the green synthesis of CuO NPs using *Ectocarpales* algal extract and their incorporation into starch/PVA electrospun nanoscaffolds for enhanced wound healing. Comprehensive characterization confirmed the formation of monoclinic-phase CuO NPs with high crystallinity, uniform dispersion within nanofibers, and improved thermal stability. The nanoscaffolds exhibited a porous, nanofibrous structure ideal for cell migration, while FT-IR and XRD analyses validated successful nanoparticle integration. In vitro wound healing assays revealed that the starch/PVA/CuO-NP nanoscaffolds significantly accelerated HaCaT keratinocyte migration, achieving near-complete wound closure (99.517%) at 100 µg/mL—outperforming both pure CuO NPs (87.517%) and algal extract (73.517%). This superior efficacy can be attributed to the synergistic effects of the nanofibrous scaffold's biomimetic architecture and the bioactive CuO NPs, which collectively promote cellular proliferation and tissue regeneration. These findings highlight the potential of algae-mediated CuO NPs and their polymer nanocomposites as advanced wound dressings. Future studies should focus on in vivo validation and mechanistic insights into their regenerative properties, paving the way for clinical translation in chronic wound management.

Ethical Declaration: Not applicable for this study.

Funding: Not available for this study.

Conflicts of Interest: The authors declare no conflicts of interest.

Data Availability Statement: The full dataset of physiochemical characterization associated with this work is published in Mendeley Data [Dataset] Structural and functional profiling of starch-polymer nanoscaffolds enhanced with *Ectocarpales*-derived biogenic copper oxide nanoparticles (DOI: 10.17632/m7jzmb7mr9.1). Disclosure: The material characterization data and figures (e.g., UV, SEM, FTIR, XRD, TGA, Zeta Potential and particle sizer) presented here were generated from a common dataset and are being reused across multiple related studies on nanomaterials. All biological analyses and conclusions are original to each manuscript.

REFERENCES

1. Ganesan A, Kumar NG, Natarajan PM. Anticancer activity of silver nanoparticles synthesized from aqueous leaf extract of Solanum trilobatum (Purple fruit pea eggplant) on human oral cancer cells. Journal of Herbmed Pharmacololgy. 2024; 13(2): 260-268.
2. Umapathy V, Dhanavel A, Kesavan R, Natarajan PM, Bhuminathan S, Vijayalakshmi P. Anticancer Potential of the Principal Constituent of Piper nigrum, Piperine: A Comprehensive Review. Cureus. 2024; 16(2): e54425.
3. Natarajan PM, Bhuminathan S, Rajan R, Bindu K, Loganathan K, Veerakumar R. The Crucial Role of Smoking Cessation in Preventing Oral Cancer. Journal of Pharmacy and Bioallied Sciences. 2024; 16(5): S4245-S4247.
4. Umapathy VR, Swamikannu B, Natarajan PM, Devi R, Nandini MS, Vimalarani, Vijayalakshmi P. In Silico Molecular Docking of Ocimum sanctum Phytochemicals: Targeting Key Biomarkers in Oral Cancer. Journal of Pharmacy and Bioallied Sciences. 2024; 16(5): S4792-S4799.
5. Natarajan PM, Umapathy VR. Role of transcriptomics in the study of oral cancer. Frontiers in Oral Health. 2025; 6:1524364.
6. Swamikannu B, Umapathy VR, Natarajan PM, Nandini MS, Stylin AGSQ, Vimalarani V, Rajinikanth S. Unlocking the Therapeutic Benefits of Artemisia Annua: A Comprehensive Overview of its Medicinal Properties. Journal of Pharmacy and Bioallied Sciences. 2024; 16(5): S4248-S4253.
7. Kunamalla R, Panagal M, Palanisamy CP. Biogenic synthesis and fabrication of starch/PVA/CuO electrospun nanoscaffolds from Sargassum ilicifolium (brown marine macroalgae) extract for anticancer activity on HT-29 and MCF-7 cancer cells. Biocatalysis and Agricultural Biotechnology. 2026; 72: 103923.

8. Pei J, Govindaraj H, Sivaramakrishnan R, Kanniappan GV, Pandurangan V, Dhayalan VK, Mironescu M, Mironescu ID, Jayaraman S, Palanisamy PC. Sustainable fabrication of biopolymer-based (starch/PVA) nanoscaffolds loaded with green-synthesized CuO nanoparticles from Sargassum wightii (marine macroalgae): Cytocompatibility and antioxidant activity. Biomaterials Advances. 2026; 182: 214660.
9. Pei J, Perumal NC, Meng P, Long Q, Palanisamy CP. Extracellular vesicle-based biosensors for Alzheimer's disease: A new frontier in precision diagnostics. Ageing Research Reviews. 2026; 113: 102904.
10. Shree P, Sivaramakrishnan R, Kanniappan GV, Pandurangan V, Jayaraman S, Dhayalan VK, Mironescu M, Mironescu ID, Palanisamy CP. Antioxidant and biocompatible CuO-starch/PVA nanoscaffolds via ultrasonic green synthesis using Turbinaria conoides (brown marine macroalgae). Medicine in Drug Discovery. 2025; 28: 100238.
11. Gong J, Lin J, Guan T, Pei J, Palanisamy CP, El-AtyFrom AMA. selenium tolerance to nanoplastic antagonism: Comprehensive characterization of L. casei SNUT1 and its extracellular vesicle–nanoselenium complex. Food Bioscience. 2025; 74: 107749.
12. Poochi SP, Sundarraj R, Raju MV, Chandrasekaran MK, Ahalliya RM, Palanisamy CP, Kanniappan GV, Kondapavuluri BK, Thiruvengadam M. Harnessing Nature: Computational and Experimental Insights Into Ipomoea obscura Metabolites for Bladder Cancer Therapy. Chemistry and Biodiversity. 2025; 0: e00909.
13. Dugganaboyana GK, Kannankumar MKG, Shivaramakrishna S, Raju MV, Chandrasekaran MK, Ahalliya RM, Panneerselvam N, Palanisamy CP, Kanniappan GV. Phytochemical insights, antioxidant activity and therapeutic potential of Cassia senna against prostate cancer in Wistar albino rats. Discover Applied Sciences. 2025; 7:1206.
14. Natarajan SR, Krishnamoorthy R, Alshuniaber MA, Gatasheh MK, Rajagopal P, Veeraraghavan VP, Palanisamy CP, Jayaraman S. KDM1A Facilitates Oncogenic Potential in Colorectal Cancer Progression Through the Activation of AXIN/GSK3β/β-Catenin Signaling Pathways: Evidence From Integrated Transcriptomics and In Vitro Studies. The Journal of Gene Medicine. 2025; 27(11): e70053.
15. Guan T, Gong J, Lin J, Palanisamy CP, Jinjin Pei J, El-Aty AMA. Machine learning-driven multimodal optimization of selenium biotransformation and flavor profiling in fermented apple–Yacon functional beverages. Innovative Food Science & Emerging Technologies. 2025; 105: 104198.
16. Natarajan SR, Krishnamoorthy R, Alshuniaber MA, Alsulami TS, Gatasheh MK, Rajagopal P, Palanisamy CP, Govindan R, Veeraraghavan VP, Jayaraman S. ABCE1 facilitates tumour progression via aerobic glycolysis and inhibits cell death in human colorectal cancer cells through the p53 signalling pathway. Scientific Reports. 2025; 15: 24674.
17. Huang Y, Guo H, Liu Y, Jin W, Palanisamy CP, Pei J, Oz F, El-Aty AMA. Effects of Natural Polysaccharides on the Gut Microbiota Related to Human Metabolic Health. Molecular Nutrition & Food Research. 2025; 69:e202400792.
18. Poornima K, Meenakshi K.C, Manikandan V.R, Shankari G, Prabhu D, Rathi M.A, Palanisamy CP, Balaji R, Gopalakrishnan V.K. Exploring the anticancer potential of Jerantinine A from Tabernaemontana coronaria against prostate, breast, and ovarian cancers: A computational approach. Journal of Complementary and Integrative Medicine, 2025 22(2): 363–372.
19. Palanisamy CP, Poompradub S, Sansanaphongpricha K, Jayaraman S, Subramani K. Faridah Sonsudin gGreen synthesis of Nigella sativa-mediated silver nanoparticles for enhanced antibacterial activity and wound healing: Mechanistic insights and biomedical applications. Environmental Nanotechnology, Monitoring & Management. 2025; 24: 101085.
20. Surendran N, Raju MV, Chandrasekaran MK, Ahalliya RM, Palanisamy CP, Chandrasekaran G, Kanniappan GV. Physicochemical characterization of starch from Maranta arundinacea L.(arrowroot) rhizomes and its inhibition of COX-2: In vivo validation. Bioactive Carbohydrates and Dietary Fibre. 2025; 33: 100465.
21. Kannappan P, Chandrasekaran MK, Raju MV, Gopalakrishnan S, Dhamodharan P, Ahalliya RM, Palanisamy CP, Raju B, Kanniappan GV. Exploring the anticancer potential of Jerantinine A from Tabernaemontana coronaria against prostate, breast, and ovarian cancers: a computational approach. Journal of Complementary and Integrative Medicine. 2025; 22(02): 363-372.
22. Pei J, Kumarasamy RV, Jayaraman S, Kanniappan GV, Long Q, Palanisamy CP. Quercetin-functionalized nanomaterials: Innovative therapeutic avenues for Alzheimer's disease management. Ageing Research Reviews. 2025; 104: 102665.
23. Jayaraman S, Prasad M, Natarajan SR, Krishnamoorthy R, Alshuniaber MA, Gatasheh MK, Veeraraghavan VP, Rajagopal P, Palanisamy CP. Molecular mechanisms underlying the effects of beta-sitosterol on TGF-β1/Nrf2/SIRT1/p53-mediated signaling in the kidney of a high-fat diet and sucrose-induced type-2 diabetic rat. Chemico-Biological Interactions. 2025; 411: 111443.
24. Huang Y, Guo H, Liu Y, Jin W, Palanisamy CP, Pei J, Oz F, El-Aty AMA. Effects of Natural Polysaccharides on the Gut Microbiota Related to Human Metabolic Health. Molecular Nutrition & Food Research. 2025; e202400792.
25. Prabhakaran P, Palanisamy CP, Shanmugam A, Damodharan P, Swaminathan H, Devaraj D, Ahalliya RM, Kanniappan GV. Isolation, structural characterization, and molecular docking studies on the bioactive compound from n-Hexane extract of Emilia sonchifolia (L.) DC against the pancreatic cancer target Aurora 2 Kinase. Journal of Complementary and Integrative Medicine. 2024; 22(1): 0290.
26. Jiang H, Kumarasamy RV, Pei J, Raju K, Kanniappan GV, Palanisamy CP. Integrating engineered nanomaterials with extracellular vesicles: Advancing targeted drug delivery and biomedical applications. Frontiers in Nanotechnology. 2024; 6: 1513683.
27. Guo H, Liu Y, Wan T, Song D, Palanisamy CP, Geng J, Pei J, Özmen S, El-Aty AMA. Toward personalized cancer management: Role of precision nutrition–diet interventions. Journal of Functional Foods. 2024; 123: 106584.
28. Natarajan SR, Krishnamoorthy R, Alshuniaber MA, Al-Anazi KM, Farah MA, Rajagopal P, Palanisamy CP, Veeraraghavan VP, Jayaraman S. Identification of FOXM1 as a novel protein biomarker and therapeutic target for

colorectal cancer progression: Evidence from immune infiltration and bioinformatic analyses. International Journal of Biological Macromolecules. 282 (Part 4): 137201.
29. Rajendran MS, Jayaraman S, Khan JM, Jasmine S, Prabhakaran RK, Raju MV, Chandrasekaran MK, Ahalliya RM, Kannappan P, Palanisamy CP, Kanniappan GV. Investigating the colon toxicity and carcinogenic role of monosodium glutamate compared with Dimethylhydrazine in male Wistar rats: Exploring the link to childhood colon cancer risk. Journal of King Saud University - Science. 2024; 36(11): 103507.
30. Kumarasamy RV, Natarajan PM, Umapathy VR, Roy JR, Rab SO, Saeed M, Panagal M, Mironescu M, Srinivasan GP, Palanisamy CP. Clinical Applications and Therapeutic Potentials of Advanced Nanoparticles: A Comprehensive Review on Completed Human Clinical Trials. Frontiers in Nanotechnology. 2024; 6:1479993.
31. Jin W, Pei JJ, Roy JR, Jayaraman S, Ahalliya RM, Kanniappan GV, Mironescu M, Palanisamy CP. Comprehensive review on single-cell RNA sequencing: A new frontier in Alzheimer's disease research. Ageing Research Reviews. 2024; 274: 102454.
32. Pei J, Palanisamy CP, Jayaraman S, Natarajan PM, Umapathy VR, Roy JR, Panagal M, Jayaraman S. Curcumin-loaded polymeric nanomaterials as a novel therapeutic strategy for Alzheimer's disease: A comprehensive review. Ageing Research Reviews. 2024; 99: 102393.
33. Pei J, Palanisamy CP, Jayaraman S, Natarajan PM, Umapathy VR, Roy JR, Thalamati D, Ahalliya RM, Kanniappan GV*, Mironescu M. A comprehensive review on starch-based Sustainable Edible Films Loaded with Bioactive Components for Food Packaging. International Journal of Biological macromolecules. 2024; 274 (Part-1): 133332.
34. Palanisamy CP, poompradub S, Sansanaphongpricha K, Subramani K, Sonsudin F. Increased expression levels of PDGF and VEGF magnify the wound healing potential facilitated by biogenic synthesis of silver nanoparticles. Nano-Structures & Nano-Objects. 2024; 39: 101236.
35. Pei J, Palanisamy CP, Jayaraman S, Natarajan PM, Umapathy VR, Roy JR, Thalamati D, Ahalliya RM, Kanniappan GV, Mironescu M. Proteomics Profiling of Extracellular Vesicle for Identification of Potential Biomarkers in Alzheimer's Disease: A Comprehensive Review. Ageing Research Reviews. 2024; 99: 102359.
36. Xi J, Wang T, Xian P, Liu X, Du M, Yang H, Palanisamy CP, Lin W, Long Q. Proteomic insights uncover enhanced neurotherapeutic potential in conditioned mesenchymal stem cell-derived extracellular vesicles. Extracellular Vesicle. 2024; 3: 100037.
37. Natarajan PM. Dental Bioinformnatics-Current Scope and Future perspectives. Research Journal of Pharmacy and Technology. 2022;15(5):2351-6.
38. Vidhyarekha U, Natarajan PM, Bhuminathan S, Sabarinathan J, Suba R, Vijayalakshmi P. Role of artificial intelligence in Oral Cancer. Advances in Public Health. 2024. 2024: 3664408.
39. Ganesan A, Kumar NG, Natarajan PM, Gauthaman J. Automated classification of elongated styloid processes using deep learning models-an artificial intelligence diagnostics. Frontiers in Oral Health. 2025; 5: 1424840.
40. Umapathy VR, Natarajan PM, Swamikannu B. Regenerative Strategies in Dentistry: Harnessing Stem Cells, Biomaterials and Bioactive Materials for Tissue Repair. Biomolecules. 2025; 15: 546.
41. Natarajan PM, Umapathy VR, Murali A, Swamikannu B. (2022). Computational Simulations of Identified marine-derived Natural Bioactive Compounds As Potential Inhibitors of Oral Cancer. Future Science OA. 2022; 8(3).
42. Ganesan A, Kumar NG, Natarajan PM. Solanum trilobatum leaf extract-derived silver nanoparticles downregulate the PI3K/AKT/mTOR signaling pathway and attenuate oral squamous cell carcinoma cell proliferation. Journal of Herbmed Pharmacology. 2024; 13(2): 300-307.
43. Perumal MKK, Renuka RR, Subbiah SK, Natarajan PM. Artificial intelligence-driven clinical decision support systems for early detection and precision therapy in oral cancer: a mini review. Frontiers in Oral Health. 2025; 6: 1592428.
44. Ramesh E, Ganesan A, Lakshmi KC, Natarajan PM. Artificial intelligence-based diagnosis of oral leukoplakia using deep convolutional neural networks Xception and MobileNet-v2. Frontiers in Oral Health. 2025; 6: 1414524.
45. Natarajan PM. Computational Studies on Recent Congeners of Fluoroquinolones and Nitroimidazoles for Their Use in Periodontal Therapy. Journal of Pharmacy and Bioallied Sciences. 2024; 16(5): S4731-S4740.
46. Pei J, Natarajan PM, Umapathy VR, Swamikannu B, Sivaraman NM, Krishnasamy L, Palanisamy CP. Advancements in the synthesis and functionalization of zinc oxide-based nanomaterials for enhanced oral cancer therapy. Molecules. 2024; 29(11): 2706.
47. Gatasheh MK, Natarajan SR, Krishnamoorthy R, Alsulami TS, Rajagopal P, Palanisamy CP, Veeraraghavan VP, Jayaraman S. Molecular analysis to identify novel potential biomarkers as drug targets in colorectal cancer therapy: an integrated bioinformatics analysis. Molecular and Cellular Oncology. 2024; 11(1): 2326699.
48. Pei J, Yan Y, Jayaraman S, Rajagopal P, Natarajan PM, Umapathy VR, Gopathy S, Roy JR, Sadagopan CS, Thalamati D, Palanisamy CP, Mironescu M. A review on advancements in the application of starch-based nanomaterials in biomedicine: Precision drug delivery and cancer therapy. International Journal of Biological Macromolecules. 2024; 130746.
49. Pei JJ, Yan Y, Palanisamy CP, Jayaraman S, Natarajan PM, Umapathy VR, Gopathy S, Roy JR, Sadagopan JC, Thalamati D, Mironescu M. Materials-based drug delivery approaches: Recent advances and future perspectives. Green Processing and Synthesis. 2024; 13: 20230094.
50. Panneerselvam S, Viswaja K, Deepa E, Prathiba S, Rebecca FS, Nivedha RP, Rajagopal P, Veeraraghavan VP, Sridevi G, Palanisamy CP, Jayaraman S. Hypoglycemic Potential of Acalypha indica in Streptozotocin-Induced Type 2 Diabetic Rats. International Journal of Drug Delivery Technology. 2026; 16(26s):1038-1047.
51. Panneerselvam S, Viswaja K, Prathiba S, Rebecca FS, Nivedha RP, Rajagopal P, Fathima SJH, Veeraraghavan VP, Sridevi G, Palanisamy CP, Jayaraman S. Acalypha Indica Attenuates Insulin Resistance in STZ-Induced Type 2 Diabetic Male Rats: Mechanistic Study. International Journal of Drug Delivery Technology. 2026; 16(26s):1027-1037.

52. Manju NE, Natarajan A, Rebecca FS, Nivedha RP, Hemalatha R, Rajagopal P, Murali R, Veeraraghavan VP, Sridevi G, Palanisamy CP, Jayaraman S. Effect of Seendhil polyherbal formulation in attenuating type-2 diabetes in STZ-induced experimental rats. International Journal of Drug Delivery Technology. 2026; 16(26s):981-989.
53. Manju NE, Natarajan A, Rebecca FS, Nivedha RP, Hemalatha R, Rajagopal P, Murali R, Veeraraghavan VP, Sridevi G, Palanisamy CP, Jayaraman S. Molecular mechanism to identify the effects of Seendhil polyherbal preparation on IRS-1/AKT/GLUT4/NRF2-KEAP-1 mediated signaling in SFZ-induced type-2 diabetic adult male rats. International Journal of Drug Delivery Technology. 2026;16(26s):972-980.
54. Palanisamy CP, Poompradub S, Sansanaphongpricha K, Jayaraman S, Subramani K, Sonsudin F. Biosynthesis of silver nanoparticles (AgNPs) using ethanolic extract of Nigella sativa (L.) seeds promotes wound healing via PDGF and VEGF signalling pathways activation. Biocatalysis and Agricultural Biotechnology. 2023; 54: 102970.
55. Palanisamy CP, Pei JJ, Phaniendra A, Venkata AAN, Jayaraman S, Veeraragahavan VP, Sridevi G, Roy JR, Janaki CS, Thalamati D, Mironescu M, Luo Q, Chai Y, Long Q. New Strategy of Neurodegenerative Disease Treatment with Extracellular Vesicles (EVs) Derived from Mesenchymal Stem Cells (MSCs). Theranostics. 2023; 13(12):4138-4165.
56. Yadalam PK, Arumuganainar D, Natarajan PM, Ardila CM. Artificial intelligence-powered prediction of AIM-2 inflammasome sequences using transformers and graph attention networks in periodontal inflammation. Scientific Reports. 2025; 15: 8733.
57. Yadalam PK, Chatterjee S, Natarajan PM, Ardila CM. Comparison of light gradient boosting and logistic regression for interactomic hub genes in Porphyromonas gingivalis and Fusobacterium nucleatum-induced periodontitis with Alzheimer's disease. Frontiers in Oral Health. 2025; 6:1463458.
58. Natarajan PM, Bhuminathan S, Leela B, Bindu K, Loganathan K, Ramachandran V. Smoking and its Role in Oral Cancer. Journal of Pharmacy and Bioallied Sciences 16(5): S4242-S4244.
59. Yadalam PK, Natarajan PM, Ardila CM. Variational graph autoencoder for reconstructed transcriptomic data associated with NLRP3 mediated pyroptosis in periodontitis. Scientific Reports. 2025; 15: 1962.
60. Natarajan PM, Swamikannu B, Sivaraman NM, Stylin AGSQ. Prevention of Oral Cancer: A Comprehensive Guide. Journal of Pharmacy and Bioallied Sciences. 2024; 16(5): S4239-S4241.
61. Surendran N, Chandrasekaran G, Raju MV, Chandrasekaran MK, Ahalliya RM, Palanisamy CP, Kanniappan GV, Arcot R, Alharbi NS, Thiruvengadam M. Anti-inflammatory potential of ethanolic extract of Maranta arundinacea L.: Insights from COX-2 modulation and oxidative stress analysis. South African Journal of Botany. 2026; 195: 142-151.
62. Pei J, Senthilkumar MV, Hessini K, Subramaniyam S, Sivaramakrishnan R, Kanniappan GV, Jayaraman S, Palanisamy CP. Green fabrication of starch/PVA/CuO nanoscaffolds using marine macroalgae extract for enhanced anti-inflammatory activity. Sustainable Chemistry and Pharmacy. 2026; 51: 102397.
63. Balasubramanian V, Loganathan L, Muthuswamy K, Viswanathan TM, Raju MV, Chandrasekaran MK, Ahalliya RM, Poorasamy J, Palanisamy CP, Dominic S, Kanniappan GV. Anticancer therapeutic efficacy of PEGylated β-galactosidase from Aspergillus terreus in DMBA-induced breast cancer: Toxicological, molecular and histopathological evaluation in Wistar rats. International Journal of Biological Macromolecules. 2026; 360: 151856.
64. Jayaraman S, Eswaran A, Rajagopal P, Palanisamy CP, Veerakumar P, Veeraraghavan VP, Sirasanagandla SR. Neuroendocrine-associated epigenetic factors in cellular senescence: mechanisms and therapeutic implications. Biogerontology. 2026; 27(2): 64.
65. Ponnusamy B, Rajagopal P, Palanisamy CP, Veeraraghavan VP, Jayaraman S. Mechanistic Exploration of the anticancer activity of Justicia adhatoda Plant Leaf Ethanolic Extract against Colon Cancer Cells: An in silico and in vitro Approach. Asian Pacific Journal of Cancer Prevention. 2026; 27(3): 1069-1080.
66. Pei J, Saran VS, Sivaramakrishnan R, Kanniappan GV, Pandurangan V, Jayaraman S, Dhayalan VK, Mironescu M, Mironescu ID, Palanisamy CP. Ultrasonic-assisted, Sargassum ilicifolium (brown marine macroalgae)-mediated biogenic synthesis of CuO nanoparticles incorporated in starch/PVA electrospun nanoscaffolds: In vitro safety and antioxidant efficacy assessment. Bioorganic Chemistry. 2026; 173: 109679.
67. Raj MAPA, Subramaniyam S, Kanniappan GV, Jayaraman S, Palanisamy CP. Sustainable fabrication of starch/PVA/CuO electrospun nanoscaffolds from Turbinaria ornata (marine macroalgae) extract: Physicochemical characterization and antidiabetic evaluation. Kuwait Journal of Science. 2026; 53(2): 100545.
68. Pei J, Ganesh NS, Subramaniyam S, Sivaramakrishnan R, Kanniappan GV, Jayaraman S, Palanisamy CP. Sustainable fabrication of starch/PVA/CuO electrospun nanoscaffolds from Padina tetrastromatica (Brown macroalgae) extract: Physicochemical characterization and antidiabetic assessment. Sustainable Chemistry One World. 2026; 9: 100195.
69. Sakthiraj A, Sivaramakrishnan R, Subramaniyam S, Kanniappan GV, Pandurangan V, Jayaraman S, Dhayalan VK, Mironescu M, Mironescu ID, Palanisamy CP. Chemical Physics Impact. Starch/PVA electrospun nanoscaffolds loaded with ultrasonic-assisted green-synthesis of CuO nanoparticles from marine macroalgae (Gracilaria corticata) extract: Cytotoxicity and antioxidant analysis. 2026; 12: 101018.
70. Raju M, Chandrasekaran MK, Loganathan L, Ahalliya RM, Mironescu M, Mironescu ID, Palanisamy CP, Kanniappan GV. Lipid remodeling and ferroptosis in phosphatidylcholine-mediated tumor–stroma crosstalk. Frontiers in Molecular Biosciences. 2026; 13: 1742305.
71. Villagrán Z, Anaya-Esparza LM, Velázquez-Carriles CA, Silva-Jara JM, Ruvalcaba-Gómez JM, Aurora-Vigo EF, et al. Plant-based extracts as reducing, capping, and stabilizing agents for the green synthesis of inorganic nanoparticles. Resources. 2024;13(6):70.